Retrieval of Tropospheric Water Vapor Scale Height from Horizontal Turbulence Structure

Christopher S. Ruf, *Senior Member, IEEE,* and Shawn E. Beus

***Abstract*— A scale height of the vertical water vapor distribution in the troposphere is shown to be related to the rate at which the total integrated water vapor (IWV) decorrelates with horizontal separation. This relationship is based on the departure from simple Kolmogorov behavior of the turbulence structure of the IWV as the horizontal separation becomes a significant fraction of the scale height of the three dimensional (3-D) turbulence. The relationship is demonstrated by comparisons between direct measurements of the vertical water vapor distribution, by radiosondes, and coincident estimates of the horizontal turbulence structure, using the TOPEX Microwave Radiometer (TMR). This provides a new method by which to resolve some of the vertical structure of lower tropospheric water vapor from space. The turbulence structure estimator is applied to a larger body of TMR data to produce a sequence of images describing the dynamics of water vapor scale height across the tropical Pacific Ocean. The cyclical evolution of a basin scale east/west ridge of water vapor with high scale height near 5° north latitude is detected which is consistent with other observations of the Madden and Julian Oscillation. The general technique presented here should be applicable to many other existing data sets which image the horizontal distribution of IWV, e.g., those of the Defense Meteorological Satellite Program's special sensor microwave/imagers.**

I. Introduction

FREQUENT images of the absolute humidity in the air–sea boundary layer on a global scale would add significantly to understanding and accurate numerical modeling of the water vapor flux between the ocean and atmosphere [1]. Current methods for resolving the vertical distribution of water vapor in the lower troposphere from space have several important limitations. IR imagers such as the AVHRR and HIRS can estimate profiles of water vapor, but they perform more poorly near the ocean surface [2]. IR sensitivity near the surface is also severely reduced by cloud cover. Radiometers operating near the strong 183.3 GHz water vapor line are also capable of profiling water vapor. Retrieval of absolute humidity profiles near the surface using downward looking airborne observations has been reported [3]. Lutz *et al.* [3] also note, however, that retrieval performance under cloudy conditions is significantly degraded. Numerical simulations of the retrieval of relative humidity profiles at 183 GHz also suggest an undesirable sensitivity to the variability of surface emissivity, e.g., due to variable surface wind speed [4]. Thus, while both IR and millimeter measurements can provide valuable information about the vertical distribution of water vapor in the troposphere, their performance is reduced near the surface and can be adversely affected by clouds and wind.

Microwave radiometers which use the weak 22.2 GHz water vapor line are well suited for estimation of the vertically integrated water vapor content (IWV) in the atmosphere [5]–[7]. Contributions by water vapor to the brightness temperature measured near 22 GHz are only weakly dependent on height [8]. This results in estimates of IWV which are largely independent of the vertical distribution, but severely limits any direct measurement of the profile itself. In addition, IWV retrievals from space over the ocean are largely insensitive to variations in cloud cover and surface wind speed [9], [10].

Previous attempts have been made to infer information about the boundary layer humidity from radiometer measurements near 22 GHz. Liu and Niiler [11] estimate monthly mean values for the near surface specific humidity from monthly mean IWV retrievals by the scanning multichannel microwave radiometer. Their technique is based on the strong statistical correlation between these two parameters and does not represent a direct and independent measurement of the surface humidity itself. This qualification is born out by the fact that the quality of the surface retrieval degrades as the averaging time, and hence the necessary statistical correlation, is reduced [12]. Thus, their approach is quite robust with respect to clouds and wind, but suffers in temporal resolution. Schulz *et al.* [13] estimate surface humidity from brightness temperatures measured by the special sensor microwave/imager by adjusting the coefficients in its IWV retrieval to be preferentially sensitive to the water vapor nearer the ocean surface. They use the limited profile information contained in the raw brightness temperatures and combine this with the statistical correlation between the specific humidity near the surface and the integrated water vapor. This approach incorporates some additional information beyond the measurement of IWV, and so has better temporal resolution than the approach used in [11]. However, it still relies in large part on the statistical correlation between the measured integrated vapor and the desired surface parameter. For example, performance in very cloudy conditions, for which the correlation is weaker, is degraded [13].

A new retrieval technique is presented here which attempts to extract additional information about the vertical distribution of water vapor in the boundary layer from the turbulence

Manuscript received October 10, 1995; revised August 22, 1996. This work was supported in part by the TOPEX Project Office at the Jet Propulsion Laboratory, California Institute of Technology, Pasadena, under Contract 959 330. The JPL is under contract to the National Aeronautics and Space Administration.

The authors are with the Department of Electrical Engineering, The Pennsylvania State University, University Park, PA 16802 USA.

Publisher Item Identifier S 0196-2892(97)00377-X.

structure of IWV. Our intent is to incorporate the robust nature of the IWV estimates with a retrieval method which does not rely on indirect statistical correlations, but rather is based on a measurable quantity (the IWV turbulence structure) that is directly related to the shape of the water vapor profile. We begin with a brief review of those aspects of atmospheric turbulence which are pertinent here. A description of the IWV and coincident radiosonde measurements used in this study follows, along with a description of the data processing used to estimate turbulence structure from IWV and to estimate water vapor scale height from the radiosondes. Following this is a comparison between these estimates. We conclude with a sequence of images of turbulence structure across the tropical Pacific ocean.

II. Review of Atmospheric Turbulence

The point-to-point turbulence structure function for the three dimensional (3-D) water vapor density field is defined as

$$D_\rho(s) = \langle [\rho(\vec{r}) - \rho(\vec{r}+\vec{s})]^2 \rangle \tag{1}$$

where s is the magnitude of the separation between points, $\rho(\vec{r})$ is the water vapor density at $\vec{r}$, and the expectation is over all realizations of the random function $\rho(\vec{r})$. If the separation, s, is assumed to lie within the inner and outer scales of isotropic turbulence, then Kolmogorov turbulence theory predicts a relationship of the form [14]

$$D_\rho(s) = C_\rho s^\alpha. \tag{2}$$

The proportionality constant, C_ρ, is called the structure constant of the turbulence and scales according to the magnitude of the water vapor variability [15]. The power law exponent, α, is a measure of the rate at which the water vapor distribution decorrelates with separation distance. For the case of isotropic turbulence in three dimensions, $\alpha = 2/3$ [14]. If the separation, s, is larger than the outer scale (typically in the tens of meters), then (2) will not be strictly obeyed. For example, D_ρ will become independent of s at separations so widely spaced that the water vapor is essentially uncorrelated. Equation (2) can be considered a local model for the behavior of the turbulence structure in different regions of the separation, with C_ρ and α considered region dependent variables. For separations within the inner and outer scales of isotropic turbulence, $\alpha = 2/3$. For very large separations, $\alpha = 0$. In between, we expect α to decay from 2/3 to 0.

Measurements of IWV are related to $\rho(\vec{r})$ by

$$IWV(\vec{x}) = \int_0^\infty \rho(\vec{r} = (\vec{x}, z))\, dz \tag{3}$$

where $\vec{x}$ denotes the two dimensions of horizontal variability of the IWV field and z is the height. A turbulence structure function can be defined for the IWV field in the same manner as for the 3-D field, as

$$D_{IWV}(s) = \langle [IWV(\vec{x}) - IWV(\vec{x}+\vec{s})]^2 \rangle. \tag{4}$$

If the separation, s, lies within the inner and outer scales of isotropic turbulence for the water vapor field, then Kolmogorov theory predicts a relationship of the form

$$D_{IWV}(s) = C_{IWV} s^\beta \tag{5}$$

where the power law exponent is given by $\beta = 5/3$ [14]. We can locally fit measurements of $D_{IWV}(s)$ to (5) for separations beyond the outer scale. We expect β to roll off from 5/3 to 0 as s increases beyond the outer scale of isotropic turbulence to very large separations.

The behavior of β as a function of separation is also influenced by the finite vertical extent of the water vapor distribution. Even for the case of isotropic turbulence on all horizontal scales, separations which are an appreciable fraction of the vertical extent of the bulk of the water vapor will result in two dimensional (2-D) structure functions for which β is reduced below 5/3. This aspect of the dependence of β on separation has been recognized and studied by several investigators [16], [17]. Armstrong and Sramek [16] estimate the dependence of D_{IWV} on separation directly from sets of phase differences between radio interferometer pairs with the very large array in Socorro, New Mexico. They note a range of values $0.84 \leq \beta \leq 1.95$ for separations in the range 1–10 km. Kasuga *et al.* [18] also present evidence of a $\beta = 5/3$ power law dependence (for separations in the range 27–540 m) using phase differences at 22 GHz with the Nobeyama millimeter array. Treuhaft and Lanyi [17] corroborate this behavior with numerical simulations which predict a smooth, monotonic transition of β from 5/3 to 2/3 as the separation is varied from much less than to much greater than the height of a slab of water vapor which is isotropically turbulent on all scales within the slab. Note, however, that their model does not incorporate the additional roll off of β with separation due to the finite outer scale. Based on these results, we anticipate that a direct estimate of β, using IWV data, may provide some information about the scale height of the water vapor profile.

III. Radiometer and Radiosonde Observations and Processing

A. TOPEX Microwave Radiometer

The TOPEX/Poseidon satellite orbits at an altitude of 1375 km and an inclination of 67°. It has an exact repeat time of 9.9 days and is nonsun synchronous [19]. The primary objective of TOPEX is measurement of ocean surface topography using radar altimetry. TMR is included to correct for the delay of the radar signal due to tropospheric water vapor. It measures the brightness temperature in the nadir direction at 18.0, 21.0, and 37.0 GHz and estimates the path delay, PD, due to water vapor using statistical inversion [7]. Because the PD is nearly linearly proportional to the IWV [20], we will use its turbulence structure to estimate the power law dependence, β, of the water vapor distribution.

TMR data are recorded every 5.8 km along the satellite ground track. The PD estimates are spatial averages over the footprint of the TMR antenna, which measures 36 km in diameter at 21.0 GHz. Therefore, there is considerable overlap of the water vapor distributions from which the sequential estimates of PD are made. The behavior of the horizontal

turbulence structure function with overlapping spatial averaging has been considered [21]. Janssen *et al*. [21] find that the dependence of the decorrelation on separation is weaker with the overlap, as expected. In other words, the power law dependence, β, is expected to be lower. In our study here, we characterize the turbulence using sequential measurements of PD along ground tracks falling within specified time and space intervals. Specifically, the turbulence structure function is estimated by

$$\hat{D}_{PD}(s) = \frac{1}{N_s}\sum_{i=1}^{N_s}[PD(x_i) - PD(x_i+s)]^2 \tag{6}$$

where N_s is the number of pairs of PD samples present within the specified time and space interval which have a spatial separation of s. Thus, $\hat{D}_{PD}$ is estimated at integer multiples of the sampling step size $\Delta s = 5.8$ km. In practice, $\hat{D}_{PD}(s)$ will also include an uncorrelated noise term which must be estimated and removed. Specifically, the individual PD samples can be expressed as

$$PD(x_i) = \langle PD(x_i)\rangle + n_i \tag{7}$$

where n_i is modeled as zero mean, normally distributed noise which is independent for each i. Inserting (7) into (6) and considering the limiting case of the averaged summation in (6) to be an expectation operation gives

$$\begin{aligned}\hat{D}_{PD}(s) &= \langle[PD(x) - PD(x+s)]^2\rangle \\ &= D_{PD}(s) + 2\sigma_n^2\end{aligned} \tag{8}$$

where $D_{PD}(s)$ is the true turbulence structure function and σ_n^2 is the variance of the noise. The variance of the noise is expected to be relatively stationary over time since it is principally due to the additive noise in the brightness temperature measurements (i.e., the instrument ΔT), and so only needs to be determined once. We estimate σ_n^2 directly from the data in the following manner. The autocorrelation of the PD distribution can be estimated by

$$\hat{R}(s) = \frac{1}{N}\sum_{i=1}^{N}[PD(x_i)PD(x_i+s)]^2. \tag{9}$$

Inserting (7) into (9), expanding the cross-products, and passing from an averaged summation over to a true expectation gives

$$\hat{R}(s) = \begin{cases} R_t(0) + \sigma_n^2 & \text{if } s = 0 \\ R_t(s) & \text{if } s \neq 0 \end{cases} \tag{10}$$

where $R_t(s)$ is the "true" (i.e., noise free) autocorrelation function. We determine $\hat{R}(s)$ from a very large set of TMR orbits over open ocean regions. The true autocorrelation at $s = 0, R_t(0)$, is found by extrapolating $\hat{R}(s>0)$ back to $s = 0$. The variance follows as $\sigma_n^2 = \hat{R}(0) - R_t(0)$. This results in a value of $\sigma_n = 0.13$ cm, which is consistent with the TMR PD retrieval error budget described in [7]. The noise bias, $2\sigma_n^2$ in (8), is then subtracted from all estimates, $\hat{D}_{PD}(s)$, to determine $D_{PD}(s)$.

An estimate of the power law dependence, β, is made using a log/log linear regression of D_{PD} versus s

$$\log(D_{PD}(s)) = \beta\log(s) + \log(C_{PD}). \tag{11}$$

We include only estimates of $D_{PD}(s)$ over the range 11.6 km $\leq s \leq$ 29.0 km in our regression solution for β. This choice of range is motivated by a number of related factors

1) The PD distribution is not expected to obey a simple Kolmogorov turbulence model for very large separations for the reasons stated above;
2) While many of the observed structure functions did obey the Kolmogorov model $D_{PD} = C_{PD}s^{\beta}$ with a constant value for β out to well beyond 29 km (some as far out as 200–300 km), almost all of them did so out to 29 km;
3) Inclusion of D_{PD} ($s = 5.8$ km) in the regression resulted in estimates of β which were more sensitive to small variations in the noise floor, σ_n^2;
4) Preliminary comparisons between β and coincident estimates of the water vapor scale height, as measured by radiosondes, found a stronger correlation when this narrow range of separations was used to estimate β.

B. Radiosonde

Radiosondes provide a direct measure of the vertical profile of absolute humidity, $\rho(z)$. The height of the water vapor can be characterized in a number of ways. We consider the following approach. The fractional height, $H_f(f)$, is defined by

$$f = \frac{\int_0^{H_f}\rho(z)\,dz}{\int_0^{\infty}\rho(z)\,dz} \tag{12}$$

where f can vary from 0 to 100%. H_f determines the height below which a specified fraction of the total water vapor burden lies.

IV. Coincident Intercomparisons

A. Description of Database

The ongoing validation program for TOPEX/Poseidon includes daily collection of radiosonde data from 24 island launch sites which lie within 50 km of the satellite ground track [10]. The radiosondes are typically launched twice daily at 1100 and 2300 UTC. The satellite overpass times at each site are approximately uniformly distributed in time due to its nonsun synchronous orbit. For purposes of this intercomparison study, we have selected the subset of radiosonde launches which occurred within 100 min of the closest approach time of a satellite ground track, provided the distance at closest approach is less than 150 km. Corresponding TMR data are selected which lie within a specified radius of the radiosonde launch site. This radius is determined independently for each overpass so that the standard deviation of all PD samples within the radius remains approximately the same. This controls for large changes in the statistics of the turbulence over

the ensemble of data from which the turbulence structure is estimated. These time and space intervals define the set, N_s, of pairs of PD samples needed in (6) to estimate β. Typical values for N_s range from 50–150, depending on the separation spacing, s in (6), on the specific ground track of closest approach to the launch site, and on the radius used. Typical values for the radius were in the range 150–400 km and resulted in a standard deviation of the PD of 2.0–2.1 cm. This value for the standard deviation was chosen in order to guarantee a sufficiently large number of samples, N_s. This in turn imposes an effective spatial resolution on our estimate of β which is considerably larger than the TMR antenna footprint of 36 km. This problem is largely due to the nadir viewing geometry of the TMR. A cross-track or conically scanning IWV imager, such as SSM/I [22], should be able to estimate the turbulence structure function with much less degradation in spatial resolution because of its higher horizontal sampling density.

B. Intercomparison

Scatter plots of the fractional height, H_f, of the tropospheric water vapor versus the turbulence parameter β are shown in Fig. 1. Fractional heights are shown with $f = 10\%$ and 50%. In both cases, the general behavior is as expected based on the previous studies discussed above [16]–[18]. Higher values for β generally correspond to lower fractional heights. The correlation between β and H_f appears stronger for the 10% fractional height. In fact, scatter plots similar to those shown here for other fractional heights indicate that the strength of the correlation generally decreases as the fraction increases above 10%. We conjecture that this may be due to the stronger correspondence between the smaller fractional height and the thickness of the water vapor in the boundary layer. This boundary layer water vapor is better mixed and, hence, more representative of isotropic turbulence than are the higher regions of the profile. However, we emphasize at this point that the turbulence parameter, β, should not be considered a direct predictor of fractional height. Rather, it is directly related to the turbulence scale height. In this light, some of the scatter present in Fig. 1 can be attributed to the inherent decorrelation between turbulence scale height and 10% fractional height. This decorrelation could, for example, be the result of the relatively independent behavior of the water vapor within and above the boundary layer. While the bulk of the water vapor and of the PD variability and turbulence structure originates in the lower troposphere, there is also some fractional contribution to the turbulence structure from the upper troposphere.

Considering the dependence of earlier boundary layer estimators on the inherent correlation between IWV and surface humidity [11], [13], we next address the possibility that the success of our turbulence estimator is also an artifact of that correlation. A scatter plot of the 10% fractional heights presented in Fig. 1(a) versus their corresponding PDs, as determined by the TMR, is shown in Fig. 2. A strong correlation is present between the two parameters, as expected. In order to isolate the effect of this correlation on our turbulence

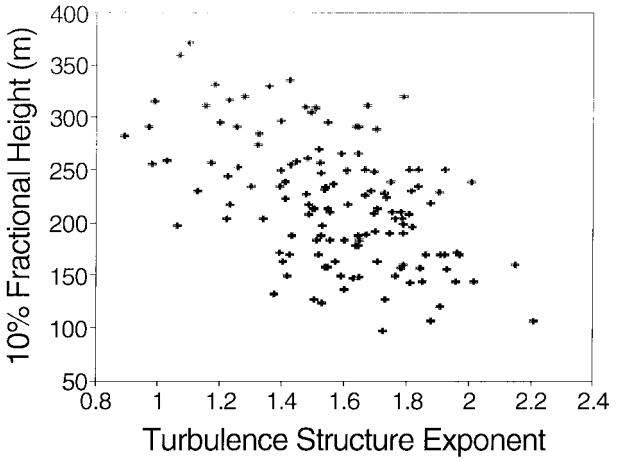

(a)

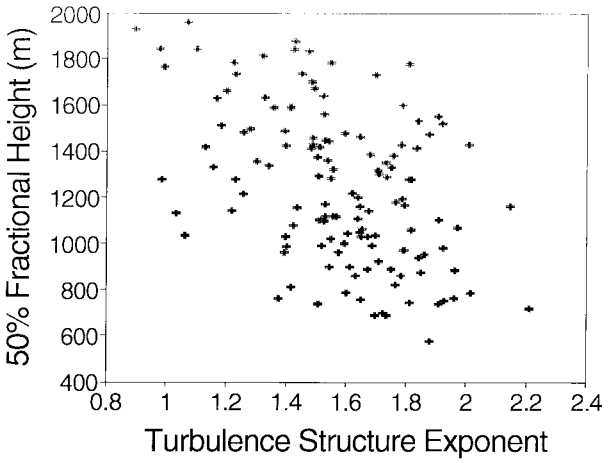

(b)

Fig. 1. The power law dependence on separation distance of the turbulence structure function for integrated water vapor is plotted against coincident radiosonde measures of the height of the water vapor profile. (a) The height of the first 10% of the integrated water vapor, and (b) The height of the first 50% of the integrated water vapor. The power law is directly related to the scale height of the turbulence, which is in turn partially correlated with these measures of height.

estimator, we consider the ability of β to predict H_f when PD is held relatively constant near its mean value. A scatter plot of the subset of 10% fractional heights for which the PD falls in the range 17.0–19.0 cm is shown in Fig. 3 versus the turbulence parameter β. Fig. 3 is a subset of Fig. 1(a) in which the effect of variations in PD has been essentially removed. The behavior of H_f with respect to β noted in Fig. 1 is still present here. Scatter plots of H_f versus β in other narrow ranges of the PD show a similar behavior. These results suggest that there is information contained in β about the vertical profile of water vapor independent of the inherent correlation between PD and near surface humidity.

A second comparison between the radiosonde fractional height and β is possible by examining a continuous time series of the two values at a common location. This has been done at a number of the radiosonde launch sites for the years 1994 and 1995. The TMR-derived estimates of β use all satellite ground tracks with closest approach points within 150 km of

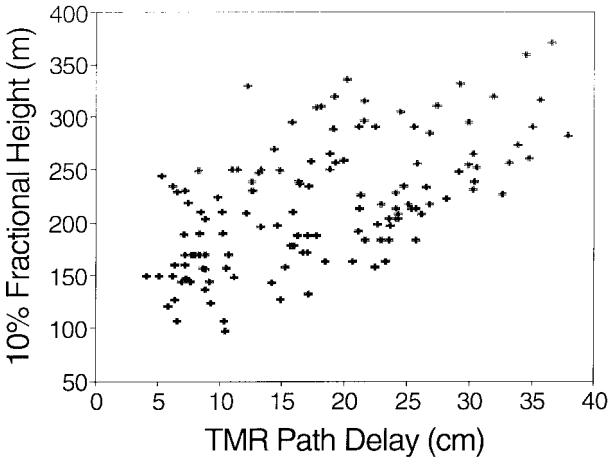

Fig. 2. Scatter plot of the 10% fractional height of water vapor versus path delay. The two parameters are highly correlated. Similar correlations between surface and integrated parameters are the basis for earlier techniques which estimate near surface humidity using microwave radiometry.

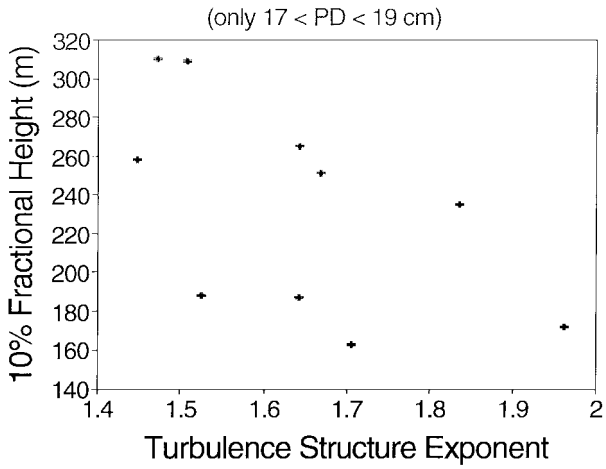

Fig. 3. Subset of Fig. 1(a) for which the path delay lies between 17.0 and 19.0 cm. This narrow filter isolates the dependence of water vapor height on the turbulence structure power law alone and indicates that the power law contains independent information about the vapor profile.

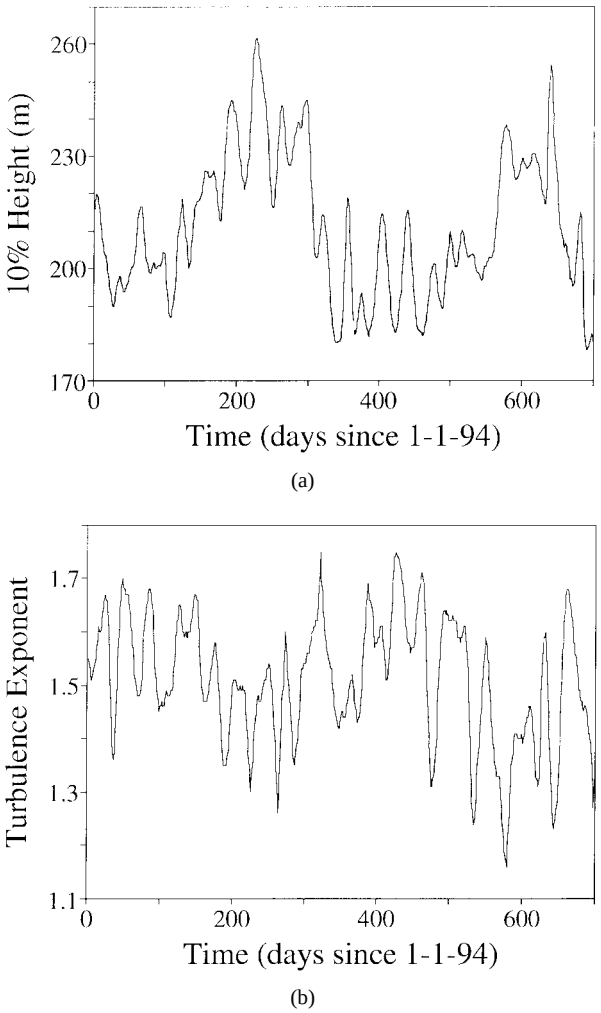

Fig. 4. Time series of radiosonde-derived 10% fractional water vapor height (a) and TMR-derived turbulence power law (b) at 166.65° east longitude, 19.28° north latitude from January 1994 to August 1995. A running ± 10 day triangular average is performed on both data sets to accommodate the 10-day orbit repeat time of the TMR. Both time series demonstrate a characteristic 40–50 day MJO.

the launch site. The β time series is smoothed by a running triangular average of ± 10 days to accommodate the sampling characteristics of the 10 day orbit repeat time. The radiosonde heights, which are generally available twice daily, have also been smoothed by a running triangular average of ± 10 days for comparison. A sample of the results is shown in Fig. 4 for the Wake Island radiosonde station (latitude 19.28° north, longitude 166.65° east). Both 10% fractional height and β time series display an oscillating behavior which is consistent with the Madden and Julian Oscillation (MJO) period of 40–50 days [23]. The phase coherence between the two time series suggests that they are responding to correlated characteristics of the water vapor profile. In addition to the similar MJO signatures, both time series also have a similar response to the seasonal variation in the height of the water vapor profile. Higher levels are noted during the 1994 and 1995 summers in both the radiosonde effective height and the turbulence scale height inferred from β.

V. Images of Tropospheric Water Vapor Scale Height

TMR derived estimates of β were also made centered on a grid of points across the tropical Pacific basin. The grid extends from 160–240° east longitude and from $-23°$ to 23° latitude, and grid points are spaced uniformly every 2°in both longitude and latitude. This results in a grid spacing of approximately 200 $\times$ 200 km. Processing at each grid point is similar to that used in the time series comparison described above, except that the radius about each point, which is used to select the ensemble of data from which the turbulence structure is estimated, has been widened to 400 km. The larger radius reduces the noise in the images while degrading the spatial resolution somewhat. The range of acceptable standard deviations of the path delay within a given radius has also been increased, from 2.0–2.1 cm in the time series comparison, to 2.0–2.3 cm here. The larger standard deviation also allows more data to be included in the ensemble, thus further reducing the noise in the image. It should be pointed out that, although the sites are spaced approximately 200 km apart, there can be

considerable overlap between sites in the particular ensemble of TMR data used to estimate β. This can be roughly viewed as a spatial smoothing effect on the images, with a typical smoothing width of diameter ≈ 600 km.

A sequence of images covering the period 14 March–22 May 1995 is shown in Fig. 5. The relatively coarse temporal resolution of 9.9 days makes much of the dynamics on smaller spatial scales difficult to interpret with confidence. However, the evolution of one prominent feature is evident. In Fig. 5(e), a ridge of high water vapor scale height (depicted in the image by lower values of β in the range 0.9–1.2) can be seen extending from 160–240° east longitude at approximately 5° north latitude. The development of this ridge over the course of the previous several weeks can be followed through Fig. 5(a)–(d). The ridge rapidly breaks up over the next few weeks, as shown in Fig. 5(f) and (g). This cyclical build up and decay of the ridge has also been observed in much of the other TMR data we have processed. The period of the cycle varies somewhat and generally lies in a range consistent with the 40–50 day MJO. A second, weaker, east/west ridge is also evident near $\approx$10° south latitude. This ridge also tends to grow and decay in cycles throughout the TOPEX mission, but is generally less well formed.

Previous indicators of the MJO have included a variety of surface and tropospheric observations from radiosondes, including air pressure, air temperature, wind speed, and water vapor mixing ratio [23]. There have also been some indications of an MJO signature in geosynchronous satellite observations of cloud cover over the tropical Pacific [24]. Comparisons between the phase of the 40–50 day periodic component of the spectra of the surface air pressure observations at various ground stations suggest that a phase front is propagating from west to east, beginning in the Indian Ocean and crossing to South America in a matter of six to seven days, with a typical phase velocity of ≈ 39 m/s [24]. This phase progression is largely confined to the region $\pm$10° latitude. The relatively short propagation time, in comparison to the 40–50 day period of the oscillation, suggests that an organized east/west feature can be expected to form across the tropical Pacific basin. This is consistent with the water vapor ridge shown in Fig. 5. However, the 9.9 day averaging effect of our data processing masks any information about the dynamics of the 6–7 day phase progression itself.

Madden and Julian [24] also suggest the presence of a much slower MJO-related propagation away from the equator in the north/south direction, with ≈ 2 m/s speed. There is some evidence of this behavior in the results presented here. For example, Fig. 5(b)–(d) in the vicinity of 200–230° east longitude and 5–23° north latitude show a series of regions with relatively high water vapor scale height apparently breaking off from the developing east/west ridge and moving to the north. The rate of progression of these cells is roughly consistent with the 2 m/s speed cited. It should be emphasized, however, that these results are preliminary. In fact, we anticipate that the application of this turbulence technique to data sets from other instruments, with faster revisit times and more complete ground coverage, will reveal much more of the dynamics associated with this MJO water vapor ridge.

A considerable amount of attention has also been directed toward modeling and understanding the causes of the MJO. Decreases in the period of the MJO to as short as 26 days, for example, have been associated with warm water events such as the El Niño-Southern Oscillation [24]. Some of the modeling results to date attempting to describe the MJO have been less than successful. Hendon and Salby [25] note, for example, that "most GCM's (global climate models) produce an analog of the MJO phase speeds nearly five times that observed." They suggest that the cause for this anomaly is most likely rooted in the insufficient vertical resolution available to the models to predict the behavior of the boundary layer water vapor. We expect that use of this turbulence retrieval technique will provide valuable information to the GCM modelers to constrain the behavior of their results in the boundary layer.

VI. Discussion

Sampling issues, especially the question of what criteria can be used to identify an acceptable ensemble of measurements from which to estimate the turbulence structure, were largely driven in our case by the relatively sparse spatial coverage and long revisit time of the TMR. These constraints resulted in spatial and temporal resolution in our basin scale images of β of approximately 600$\times$ 600 km^2 and ten days, respectively. The absolute error present in each estimate of β was found by direct numerical simulation. A representative subset of 40 locations across the tropical Pacific were selected. In each case, noisy estimates of β are made by randomly perturbing the TMR PD data with zero mean additive Gaussian noise with a standard deviation of 0.3 cm. The 0.3 cm noise level accounts for both sample-to-sample independent noise and possible short term drifts in instrument calibration [7], [21]. This was repeated several thousand times in order to determine the statistics of the error induced in β. The results indicate a standard deviation in β of 0.14 which is largely independent of the mean value of β. This error analysis suggests that noise in the estimates of β is another component of the scatter present in Fig. 1(a), in addition to the decorrelation between PD turbulence and 10% fractional height due to upper tropospheric variability noted above.

The use of horizontal turbulence statistics derived from vertically integrated measurements of IWV provides information about the scale height of the water vapor profile. While there is some correlation between the scale height of the turbulence and the fractional height, they are not necessarily sensitive to the same characteristics of a profile. Consideration of cases of weak versus strong versus multiple inversions, or of shallow versus deep versus nonexistent boundary layers, begs the question: Exactly what, from a meteorological stand point, is the turbulence scale height measuring? We suspect that this is a fairly broad and open-ended topic which will merit considerable attention in the course of the future development of this turbulence retrieval technique. Notwithstanding the need for further clarification of the turbulence scale height, the preliminary results presented here suggest that there is likely new and useful information contained in the power law dependence, β, of the turbulence structure function.

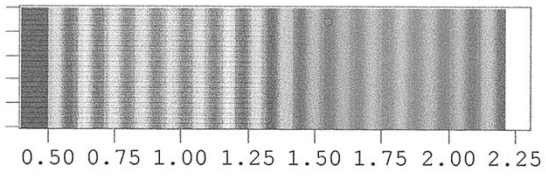

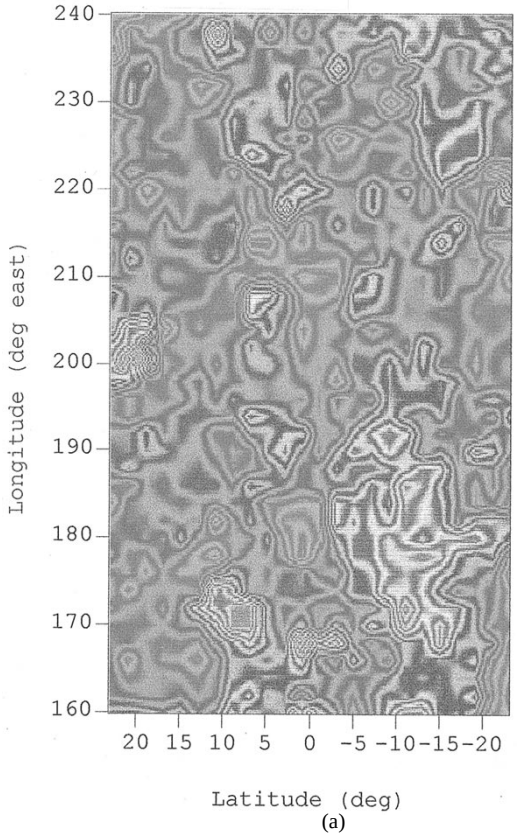

(a)

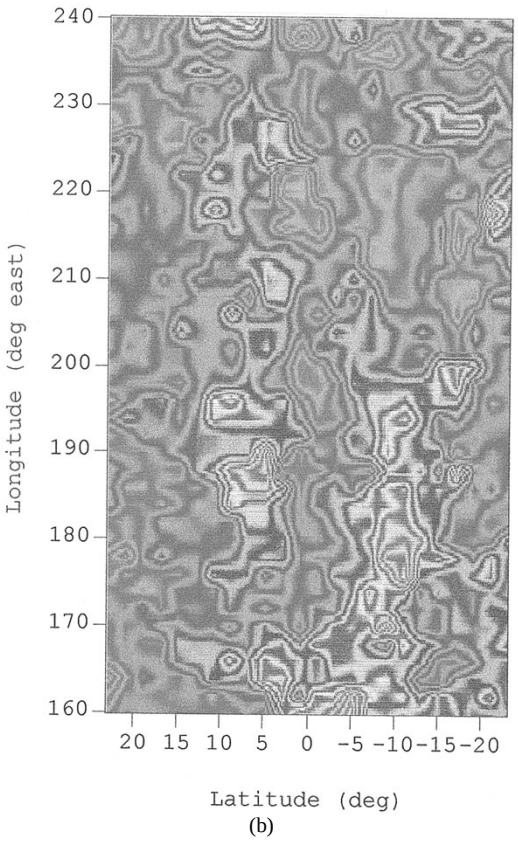

(b)

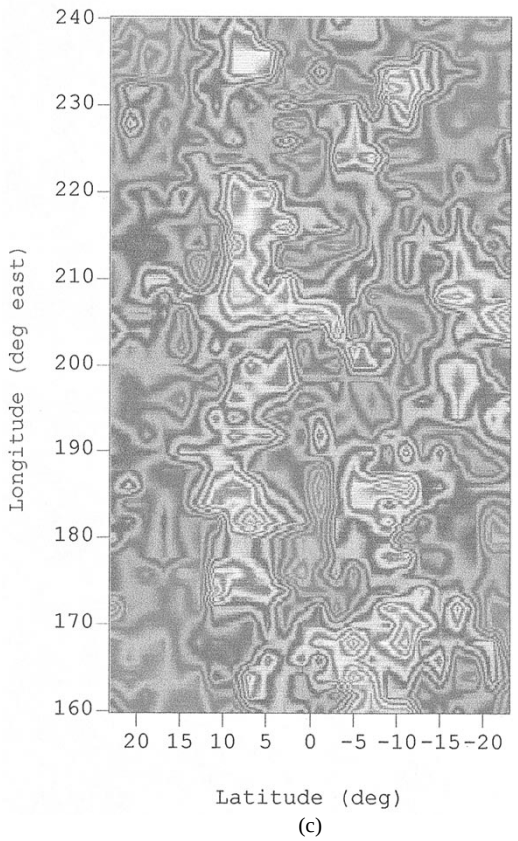

(c)

Fig. 5. TMR-derived turbulence power law images over the tropical Pacific Ocean during Spring 1995. Decreasing values correspond to an increase in the turbulence scale height of the water vapor profile. Each image is averaged over 10 days and has approximately 600 × 600 km^2 spatial resolution. Note the gradual buildup, followed by the decay, of a prominent east/west ridge of high water vapor scale height at 5° north latitude. This cycle generally repeats itself throughout much of the three year data set examined thus far. The dynamic behavior of the ridge is consistent with existing observations describing the MJO. Times for each image are: (a) 14 March–24 March; (b) 24 March–3 April; (c) 3 April–13 April.

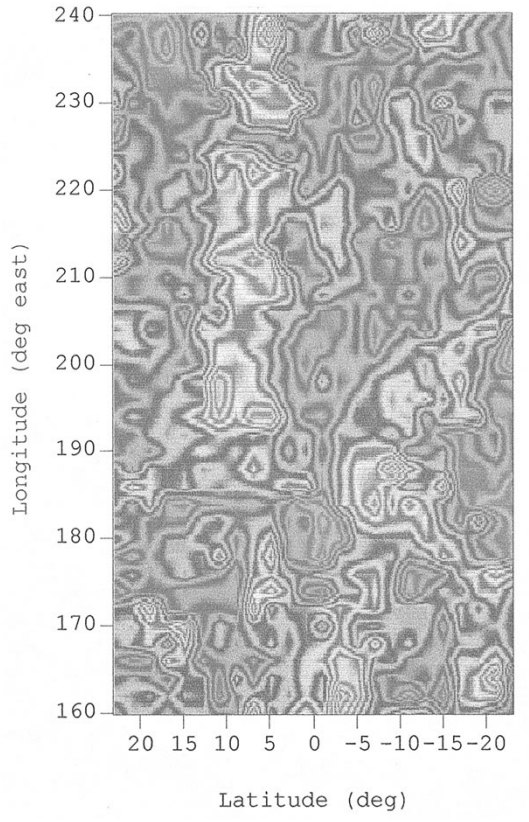

(d)

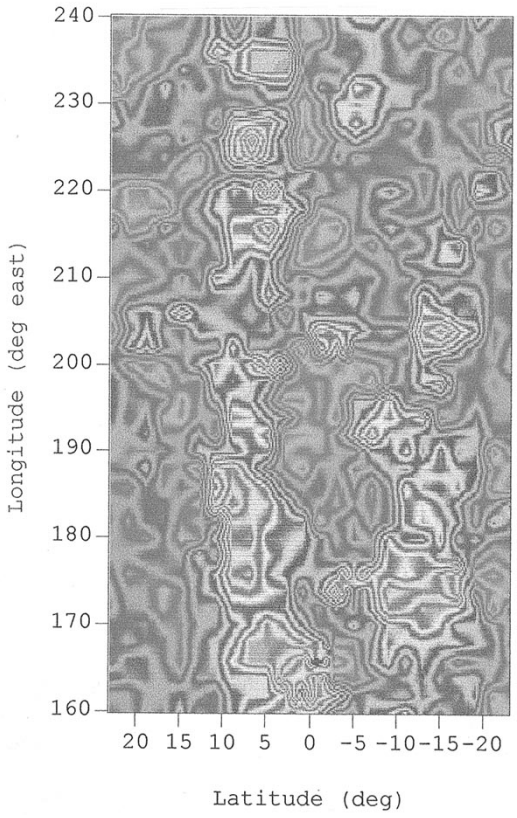

(e)

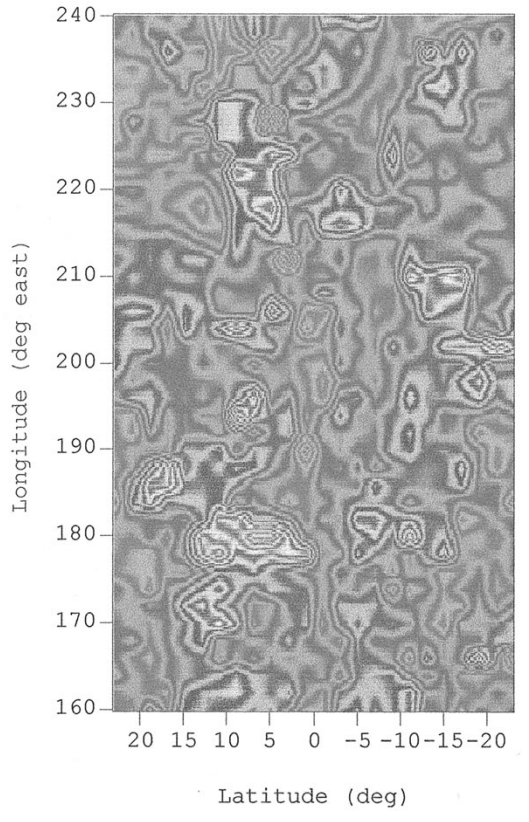

(f)

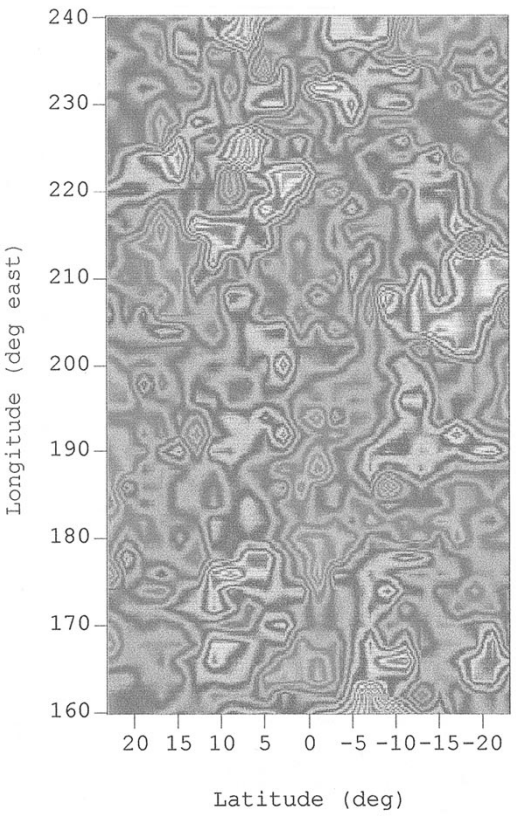

(g)

Fig. 5. (*Continued.*) Times for each image are: (d) 13 April–23 April; (e) 23 April–3 May; (f) 3 May–12 May; and (g) 12 May–22 May.

REFERENCES

[1] L. A. McMurdie and K. B. Katsaros, "Atmospheric water distribution in a midatlantic cyclone observed by the Seasat scanning multichannel microwave radiometer," *Month. Weather Rev.*, vol. 113, pp. 584–598, 1985.

[2] P. Schluessel, "Satellite-derived low-level atmospheric water vapor content from synergy of AVHRR with HIRS," *Int. J. Remote Sens.*, vol. 10, pp. 705–721, 1989.

[3] R. Lutz, T. T. Wilheit, J. R. Wang, and R. K. Kakar, "Retrieval of atmospheric water vapor profiles using radiometric measurements at 183 and 90 GHz," *IEEE Trans. Geosci. Remote Sensing*, vol. 29, pp. 602–609, July 1991.

[4] C. C. Kuo, D. H. Staelin, and P. W. Rosenkranz, "Statistical iterative scheme for estimating atmospheric relative humidity profiles," *IEEE Trans. Geosci. Remote Sensing*, vol. 32, pp. 254–260, Mar. 1994.

[5] D. H. Staelin, K. F. Kunzi, R. L. Pettyjohn, R. K. L. Poon, P. W. Rosenkranz, and J. W. Waters, "Remote sensing of atmospheric water vapor and liquid water with the Nimbus 5 microwave spectrometer," *J. Appl. Meteorol.*, vol. 15, pp. 1204–1214, 1976.

[6] T. T. Wilheit and A.T.C. Chang, "An algorithm for retrieval of ocean surface and atmospheric parameters from the observations of the scanning multichannel microwave radiometer," *Radio Sci.*, vol. 15, pp. 525–544, 1980.

[7] S. J. Keihm, M. A. Janssen, and C. S. Ruf, "TOPEX/POSEIDON microwave radiometer (TMR): III. Wet tropospheric range correction and pre-launch error budget," *IEEE Trans. Geosci. Remote Sensing*, vol. 33, pp. 147–161, Jan. 1995.

[8] E. R. Westwater, "The accuracy of water vapor and cloud liquid determination by dual-frequency ground-based microwave radiometry," *Radio Sci.*, vol. 13, pp. 667–685, 1978.

[9] J. C. Alishouse, S. A. Snyder, J. Vongsathorn, and R. R. Ferraro, "Determination of oceanic total precipitable water from SSM/I," *IEEE Trans. Geosci. Remote Sensing*, vol. 28, pp. 811–816, Sept. 1990.

[10] C. S. Ruf, S. J. Keihm, B. Subramanya, and M. A. Janssen, "TOPEX/POSEIDON microwave radiometer performance and in-flight calibration," *J. Geophys. Res.*, vol. 99, pp. 24915–24926, 1994.

[11] W. T. Liu and P. P. Niiler, "Determination of monthly mean humidity in the atmospheric surface layer over oceans from satellite data," *J. Phys. Ocean.*, vol. 14, pp. 1451–1457, 1984.

[12] G. Marchuk, K. Kondratyev, and V. Kozoderov, *Earth Radiation Budget: Key Aspects*. Moscow, Russia: Nauka, 1990.

[13] J. Schulz, P. Schluessel, and H. Grassl, "Water vapor in the atmospheric boundary layer over oceans from SSM/I measurements," *Int. J. Remote Sensing*, vol. 14, pp. 2773–2789, 1993.

[14] V. I. Tatarskii, *Wave Propagation in a Turbulent Medium*. New York: Dover, 1961.

[15] S. B. S. S. Sarma and P. K. Pasricha, "Measurements of the radio refractive index structure parameter C_n^2 with a microwave refractometer in tropical latitudes," *Aust. J. Phys.*, vol. 42, pp. 573–580, 1989.

[16] J. W. Armstrong and R. A. Sramek, "Observations of tropospheric phase scintillations at 5 GHz on vertical paths," *Radio Sci.*, vol. 17, pp. 1579–1586, 1982.

[17] R. N. Treuhaft and G. E. Lanyi, "The effect of the dynamic troposphere on radio interferometric measurements," *Radio Sci.*, vol. 22, pp. 251–265, 1987.

[18] T. Kasuga, M. Ishiguro, and Ryohei Kawabe, "Interferometric measurement of tropospheric phase fluctuations at 22 GHz on antenna spacings of 27 and 540 m," *IEEE Trans. Antennas Propagat.*, vol. 34, pp. 797–803, 1986.

[19] G. Carlisle, A. DiCicco, H. M. Harris, A. Salama, and M. Vincent, "TOPEX/Poseidon project mission plan," Document D-6862, Rev. C, Jet Propulsion Lab., Pasadena, CA, 1991.

[20] G. Elgered, "Tropospheric radio path delay from ground-based microwave radiometry," *Atmospheric Remote Sensing by Microwave Radiometry*, M.A. Janssen, Ed. New York: Wiley, 1993, ch. 5.

[21] M. A. Janssen, C. S. Ruf, and S. J. Keihm, "TOPEX/POSEIDON microwave radiometer (TMR): II. Antenna pattern correction and brightness temperature algorithm," *IEEE Trans. Geosci. Remote Sensing*, vol. 33, pp. 138–146, Jan. 1995.

[22] J. P. Hollinger, J. L. Pierce, and G. A. Poe, "SSM/I instrument evaluation," *IEEE Trans. Geosci. Remote Sensing*, vol. 28, pp. 781–790, Sept. 1990.

[23] R. A. Madden and P. R. Julian, "Description of global-scale circulation cells in the tropics with a 40–50 day period," *J. Atmos. Sci.*, vol. 29, pp. 1109–1123, 1972.

[24] ——, "Observations of the 40–50 day Tropical Oscillation—A Review," *Month. Weather Rev.*, vol. 122, pp. 814–837, 1994.

[25] H. H. Hendon and M. L. Salby, "The life cycle of the Madden–Julian oscillation," *J. Atmos. Sci.*, vol. 51, pp. 2225–2237, 1994.

Christopher S. Ruf (S'85–M'87–SM'92) received the B.A. degree in physics from Reed College, Portland, OR, in 1982 and the Ph.D. degree in electrical and computer engineering from the University of Massachusetts, Amherst, in 1987.

From 1983 to 87 he worked as a Research Assistant and continued during 1987–1988 as a Visiting Professor and Research Engineer, all with the Microwave Remote Sensing Laboratory at UMass. His research involved microwave radiometer instrumentation and data inversion in atmospheric and surface applications. He then joined the technical staff at NASA's Jet Propulsion Laboratory in 1988. While at JPL, his work involved the TOPEX Microwave Radiometer and ground based atmospheric radiometry. He left JPL to join the faculty in the Department of Electrical Engineering, The Pennsylvania State University, in 1992. His current research activities include participation in the TOPEX/Poseidon and GEOSAT follow-on flight missions, ground based atmospheric radiometry, synthetic aperture interferometric radiometry, and millimeter wave propagation studies for the remote sensing of precipitation.

Dr. Ruf is an Associate Editor for *Radio Science* and a past Associate Editor of the University Profiles column in the IEEE Geoscience and Remote Sensing Society Newsletter. He is a member of the AGU and Commission F of URSI.

Shawn E. Beus received the B.S. degree in electrical and computer engineering and the B.A. degree in Japanese from Brigham Young University in 1994 and the M.S. degree in electrical engineering from The Pennsylvania State University, University Park, in 1996. His M.S. thesis topic addressed the use of horizontal turbulence structure to infer tropospheric water vapor scale height from observations by the TOPEX Microwave Radiometer.

He is currently with Hewlett Packard, Colorado Springs, CO.